UC Irvine
UC Irvine Previously Published Works

Title

Visual and Contextual Modeling for the Detection of Repeated Mild Traumatic Brain Injury

Permalink

Journal

ISSN

Authors

Bianchi, Anthony
Bhanu, Bir
Donovan, Virginia
et al.

Publication Date

2014

DOI

Peer reviewed

Visual and Contextual Modeling for the Detection of Repeated Mild Traumatic Brain Injury

Anthony Bianchi*, Bir Bhanu, *Fellow, IEEE*, Virginia Donovan, and Andre Obenaus

Abstract—Currently, there is a lack of computational methods for the evaluation of mild traumatic brain injury (mTBI) from magnetic resonance imaging (MRI). Further, the development of automated analyses has been hindered by the subtle nature of mTBI abnormalities, which appear as low contrast MR regions. This paper proposes an approach that is able to detect mTBI lesions by combining both the high-level context and low-level visual information. The contextual model estimates the progression of the disease using subject information, such as the time since injury and the knowledge about the location of mTBI. The visual model utilizes texture features in MRI along with a probabilistic support vector machine to maximize the discrimination in unimodal MR images. These two models are fused to obtain a final estimate of the locations of the mTBI lesion. The models are tested using a novel rodent model of repeated mTBI dataset. The experimental results demonstrate that the fusion of both contextual and visual textural features outperforms other state-of-the-art approaches. Clinically, our approach has the potential to benefit both clinicians by speeding diagnosis and patients by improving clinical care.

Index Terms—Brain injury, contextual modeling, magnetic resonance imaging (MRI), textural modeling.

I. INTRODUCTION

MILD traumatic brain injury (mTBI) annually affects millions of people within the United States [1]. This is due to events, such as sports, military (blast), automobile accidents, assaults, and falls. There are many short and long term symptoms associated with mTBI including loss of memory, loss of reasoning, neuropsychiatric alterations including decrements in social interactions [2]. Recently, there has been increased focus on the potential effects of repeated mTBI as this may result in exacerbation of ongoing tissue pathology and neurological deficits. In extreme cases, second impact syndrome can occur in which a subsequent injury is sustained within hours to weeks of the first. This may result in catastrophic swelling of brain which may ultimately lead to death or the effects similar to a severe TBI [3].

Currently, neurological injuries are evaluated using the Glasgow Coma Scale (GCS) which evaluates a patient's consciousness level through his/her ability to respond to motor, verbal and visual stimuli. Other qualitative factors are used to assess the effects of TBI, including loss of consciousness, loss of memory, alteration in mental status, focal neurological deficits, and visual assessment of neuroimaging studies when performed. However, visual assessment of neuroimaging is subject to poor inter-rater reliability and may not be sensitive enough to detect mild injuries, which often show subtle or no symptoms. The clinical definitions for diagnosis of mTBI have been recently clarified [4]. If GCS abnormalities are observed, computed tomography (CT) or MR imaging is used, depending on the severity of presumed injury, to assist in diagnosis though quantitative measures are not routinely used in the clinic. However, clinical studies assessing potential quantitative methods suggest that this type of analysis can improve detection and treatment of mild injuries.

In clinical studies and those using experimental models of TBI, manual quantitative analysis has been used to evaluate TBI in MRI [5]–[7]. These manual studies have sought to identify the location and size of a lesion from MRI with correlative histology and assessment of long term neurological effects. However, manual detection of lesions in mTBI is very difficult and often requiring 1) hours per scan for manual region-of-interest analysis, 2) a trained operator to improve inter- and intra-rater reliability, 3) large data sets for statistically sound analysis but this is not feasible as it becomes resource intensive, and 4) multi-modal inputs as mild or subtle alterations on MR images are often difficult to identify (low contrast). Further consistency in manual detection is a problem with both inter- and intr-aoperator variability. This low contrast appearance on MRI exacerbates the consistency in manual evaluation as individuals interpret presumed abnormalities differently, despite strict protocols, leading to large inter-operator variations. Fig. 1 illustrates the low contrast appearance. This variability is even present in higher contrast images, such as tumor size quantification [8]. Partial volume effects along with neighboring anatomical regions can affect adjacent voxels making them seem to be of a different class [9]. Operator fatigue also plays a large role since manual detection can take a long time to analyze. However, manual segmentation is still considered the "gold standard" and automated algorithms are routinely compared to this standard.

On structural MR, gross tissue abnormalities, such as extravascular blood and edema (increased water content), can be identified in moderate to severe TBI; but these features are often

*A. Bianchi is with the Center for Research in Intelligent Systems, University of California, Riverside, CA 92521 USA (e-mail: abianchi@vislab.ee.ucr.edu).
B. Bhanu is with the Center for Research in Intelligent Systems, University of California, Riverside, CA 92521 USA (e-mail: bhanu@cris.ucr.edu).
V. Donovan is with the Cell, Molecular and Developmental Biology, University of California, Riverside, CA 92521 USA (e-mail: virginia.donovan@ucr.edu).
A. Obenaus is with the Department of Pediatrics, Radiology, Loma Linda University, Loma Linda, CA 92354 USA (e-mail: aobenaus@llu.edu).
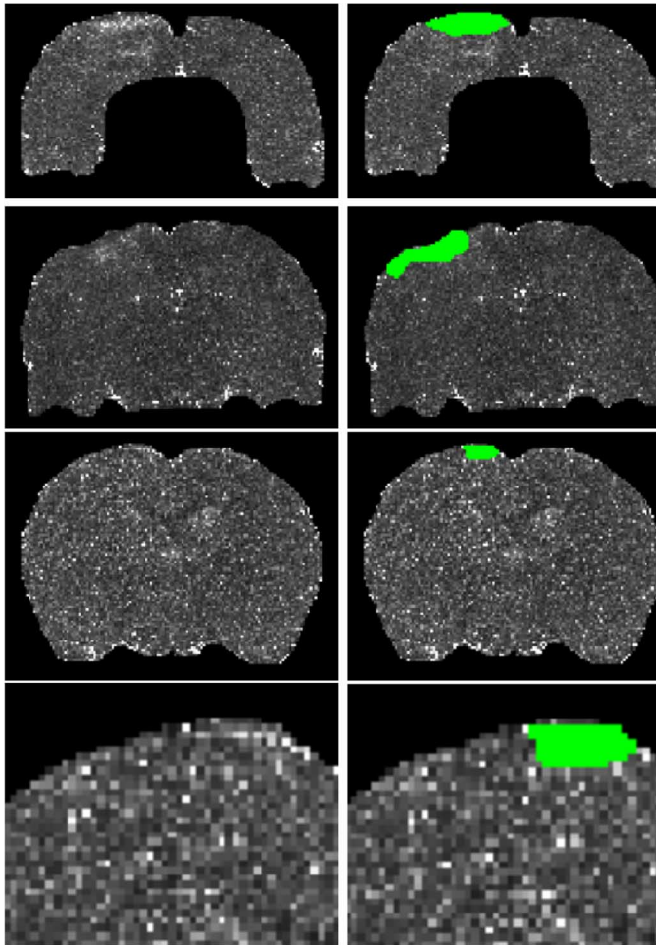
Fig. 1. Examples of mTBI lesions in a rat (mildly controlled cortical impact model for an MRI T2 map). Left column: Original coronal slices. Right column: Manually drawn lesion regions. The last row is the expanded view of the row above it. Note the texture changes in the manually drawn regions.

not present (or little) on mTBI MR data. While CT is typically used in the initial assessment of head injuries and to identify extra vascular blood in the brain, new emerging technique, such as susceptibility weighted imaging (SWI), are even more sensitive to micro-hemorrhages [10]. T2-weighted imaging (T2WI) and the resultant T2 maps are routinely used to identify structural changes, edema and tissue relaxation properties. In experimental models of TBI, T2 maps are used to identify and quantify regions of both edema (high T2 values) and extravascular blood (low T2 values). MRI T2 maps have been used for manual quantitative analysis of TBI [11]. However, edema, particularly in mTBI, can be subtle and transient further making identification of putative injury difficult. We have chosen to use T2 maps in this study due it its ability to find edema and blood in a single modality. Having a single modality decreases computation time and imaging time.

The key questions associated with detection of mTBI lesions are: single versus multiple lesions and their locations; single/ multiple lesions over time; focal versus diffuse lesion; contralateral (both hemispheres) versus ipsilateral (same hemisphere); coup versus contra coup injury. For this paper, we are concerned with modeling and analysis of single/multiple injuries (contralateral) over time where the injury is modeled by a mild

control cortical impact (CCI) animal model, which only present a focal coup injury.

In the present study, we explored the ability of computer vision and learning techniques to assess subtle alterations on quantitative T2 maps after induction of mTBI. The contrast-to-noise ratio (CNR) calculated from the manually segmented detected lesions to the normal appearing brain matter in our dataset is 6 on average, where we estimated the noise variance of the lesion regions for the calculation of CNR [12].

In order to analyze such images we use a range of different models in our integrated approach that is proposed in this paper. These models include Bayesian networks (BN) for contextual modeling, support vector machines (SVMs) for discrimination of lesion versus nonlesion tissue based on visual appearance. In addition, we used Gompertz function for effective representation of lesion progression and Fourier descriptor of brain perimeter for smoothing so as to reduce the effect low resolution and noise within MR images.

The rest of this paper is as follows. Section II presents the related work and the contributions. Section III discusses the technical approach. Section IV describes the experiments and Section V provides the conclusions.

II. RELATED WORK AND CONTRIBUTIONS

A. Related Work

To the best of our knowledge, there has not been another paper that has attempted to automatically detect mTBI abnormalities. Recently, a semi-automated approach [13] used an atlas based classification algorithm to detect lesions in severe TBI patients. The authors reported the use of a multi-modal MRI atlas of healthy human brains along with outlier detection to determine lesions which worked well in severe TBI due to the high contrast and large size of the lesions.

When comparing our proposed approach to previous works, other disease detections algorithms were considered. Some diseases that have been addressed by automated computer vision and image processing techniques are multiple sclerosis, tumors, and stroke. These diseases often have, on MRI, a high contrast appearance and a large injury size compared to mTBI, making them relatively less challenging to detect compared to mTBI. Table I has summarized some of the current methods utilized for lesion detection.

Some approaches are atlas based, but the results vary since they are dependent upon the atlas being used [14]. Registration is used across many disease detection algorithms since it allows for multiple subjects to be put into a common registered space. This allows for statistical lesion extraction, through outlier detection, with a known atlas. However, brain anatomy is variable even among healthy brains, which causes a distribution of values to be learned at every voxel in the atlas. Registration can cause a distortion in the MR values due to interpolations in the calculation of the registration [15], [16]. These registration distortions make mTBI lesions from T2 maps nearly indistinguishable.

Texture features have been used to increase the discriminatory potential of MRIs [17], [18]. Many different types of texture features have been used such as neighborhood statistics,

TABLE I
OVERVIEW OF CURRENT LESION DETECTION METHODS FOR MRI DATA

Paper	Basic Idea	Disease	Notes
Kruggel et al., 2008 [17]	Co-occurrence features with PCA and the distance to the cluster centers is used to make a probability map of injury.	White Matter Lesions	+ Utilizes high dimensional texture features. − Registration and assumes single cluster per class (multiple appearances are possible).
Renske de Boer et al., 2009 [14]	K-nearest neighbor for initial tissue segmentation. Gray matter is reclassified to lesion or non-lesion using the FLAIR channel.	White Matter Lesions	+ Uses known tissue location priors for misclassification. − Registration, disease specific property.
Anbeek et al., 2004 [22]	Direct KNN classification with spatial information using previously known lesions in the training set.	White Matter Lesions	+ Incorporates voxel location. Allows for neighboring voxels to be considered. − Registration. Does not scale to large data.
Zhang et al., 2011 [23]	SVM classification followed by region growing.	Tumor	+ Prior segmentation knowledge and texture features. − Registration, highly depends on first ramentation.
Sun et al., 2009 [24]	Asymmetry detection followed by classification.	Stroke	+ No prior knowledge and symmetry aided. − Problems with symmetrical lesions and textured regions.
Seghier et al., 2008 [25]	Tissue segmentation with an extra class followed by outlier detection in the gray/white matter classes.	Various	+ Tissue classification with an iteratively learned abnormal class. − Registration, smoothing cause problems with small lesions.
This Paper	SVM classification with texture features fused with a contextual disease model.	mTBI	+ Uses patient information, texture features, unimodal MRI − mTBI specific disease model.

co-occurrence matrices, fractals, and more. Recently, [19] showed, using manually drawn ROIs, that mTBI causes texture changes in the brain with features based on region histogram statistics, co-occurrence matrix and gradient measures. Texture features are also used in this paper to increase the discrimination of our unimodal dataset. Most of the other approaches use multiple MRI modalities to detect the disease signature they we are trying to measure. Having multiple modalities allows us to measure multiple tissue properties, but leads to longer imaging and subsequent analysis time. Thus, analysis using a minimal number of modalities is essential for efficient results.

Context has been an active area of research in computer vision [20], [21]. It can be used to overcome low contrast detection problems. Context is defined [20] as, "any information that might be relevant to object detection, categorization and classification tasks, but not directly due to the physical appearance of the object, as perceived by the image acquisition system." Context types that have been described include: local pixels, 2-D scene gist, 3-D geometric, semantic, photogrammetric, illumination, weather, geographic, temporal, and cultural [26]. Object recognition in natural scenes has been one of the active areas for context [27]–[31]. Many of these approaches use context for position priming, which is the process of estimating the location of the object based on the context. Context can be split into two types local and global. 1) Local context includes spatial relationships learned at the pixel/region level. It is used in conditional random fields and auto-context [32]. 2) Global context can be thought of as an estimation of the spatial location of an object. For instance, the sky usually occurs at the top of an image. Recently, Horsfield *et al.* [33] proposed using spatial priming in Multiple Sclerosis (MS) lesion detection. The spatial priors are learned directly from the data in a registered space. This approach works with MS since lesions occur regularly in white matter locations. However, using prior locations directly on mTBI data will not work since the injury can occur and progress at different sites within the brain. The proposed approach models the disease progression from any point of time in its progression.

B. Contributions

The contributions of this paper are as follows. 1) A contextual disease model based on Bayesian networks to estimate the spatial location of mTBI abnormalities. It allows for a range of contextual inputs, when the exact value (time or approximate location) is not known, which could be due to patient's memory loss. This contextual model helps to overcome the low contrast appearance of mTBI by focusing on the region of the search space that may have injury. 2) A visual model that is learned using texture features to build a probabilistic support vector machine (PSVM). The method does not require registration (it is spatially invariant), which can cause distortion. 3) A novel dataset of rat MR images is developed to follow mTBI to test the validity of the proposed model. The rat controlled cortical impact (CCI) mTBI model is used with multiple observations postinjury using T2 MRI maps to demonstrate the results. This paper is an extension of [34]. It extends the approach to repeated TBI and a more in-depth analysis of the contextual inputs is given.

III. TECHNICAL APPROACH

A. System Overview and Technical Rationale

The proposed system is a combination of a visual and contextual model. Fig. 2 shows the system diagram. A database of known mTBI MRI brain and lesion volumes with manually detected lesions and the associated contexts is used to build the model. The visual model uses 3-D texture features to build a probabilistic support vector machine that describes the lesion/normal appearing brain matter (NABM) space. The output is a probability map that is combined with the contextual model, where higher probabilities signify higher chances for a particular voxel being part of the lesion, where the lesion is an estimate of both blood and edema. If the lesion splits into multiple parts, it will still be captured since a voxel based classifier is used. SVM is a discriminative model which performs well with a large amount of data and can describe a complex decision space. With a voxel based classifier, both these conditions are satisfied.
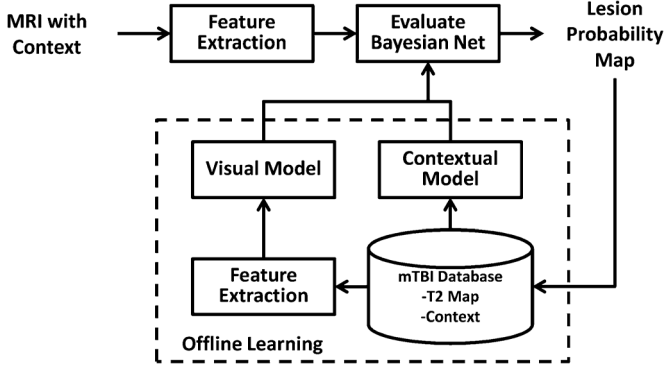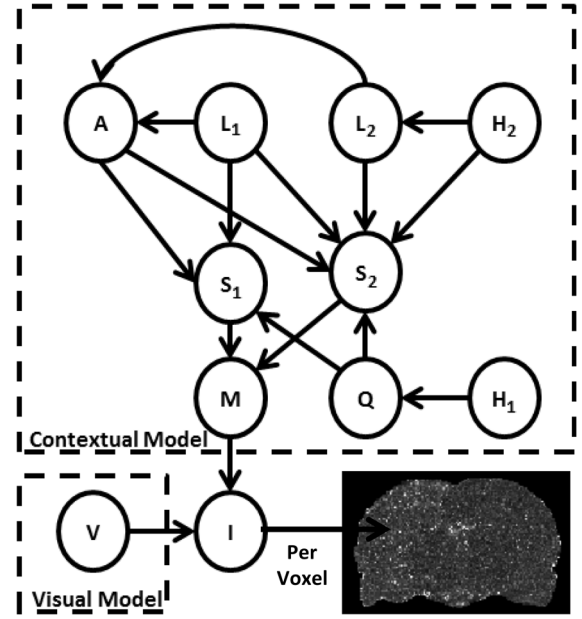
Fig. 2.   System flow diagram.

Fig. 3.   Graphical representation of the Bayesian network, showing the dependencies of random variables. Intuitive definition of distributions. A: Anatomical constraints. L_1, L_2: Central location of injury for injury one and two. H_1: Time since the first event. H_2: Time between first and second injury. Q: Volume (quantity) of injury with time. S_1, S_2: Spread for first and second injury. M: Max operator. V: Visual information. I: Estimated injury. Where I = 1 is absolute certainty of injury and I = 0 is absolute certainty of NABM.

The contextual model uses a Bayesian network (BN) to estimate the locations of the mTBI lesions (Fig. 3). This model uses knowledge about the subject, where both temporal and spatial information are used to describe the development of the disease. The BN is a generative model that is able to extrapolate based on little information when the underlying distribution assumptions hold. Generative models are used to simulate cause and effect relationships and processes, while discriminative models such as SVM do not have this ability. Our system combines the advantages from both discriminative and generative models.

When a volume enters the system the texture features are extracted and then the Bayesian net is evaluated. Contextual information is also passed to the system which includes an estimated location of the focal points of impact (L_1, L_2), time since the first injury (H_1), and time between the two injuries (H_2). These inputs can be exact (e.g., one day since injury) or a range of values (e.g., 5–14 days since injury). Each of the major steps will be described in the subsequent subsections.

B. Bayesian Net for Contextual Modeling

Modeling a joint probability distribution with many variables that interact with each other is an extremely difficult task and requires a large number of training samples. At the other extreme, naïve Bayesian learning is simple requiring a reduced numbers of samples but often poor results are observed due to features not being independent. BNs allow for a middle ground, where dependencies among variables can be modeled in a graphical manner. Directed acyclic graphs are used to represent BNs, where nodes are random variables and edges represent dependencies among random variables [35]. A BN with nodes $N_1, N_2 \ldots N_i$ results in the full joint distribution

$$p(n_1, n_2, \ldots, n_i)$$
$$= p(n_1)p(n_2|n_1) \ldots p(n_i|n_1, n_2, \ldots, n_{i-1}) \quad (1)$$
$$= \prod_{q=1}^{i} p(n_q|n_1, n_2, \ldots, n_{i-1}). \quad (2)$$

The properties of the BN allows for a node to only depend on its parents' values, so the joint distribution can be rewritten as

$$= \prod_{q=1}^{i} p(n_q|\text{parents}(N_i)). \quad (3)$$

A node in a BN is only conditional on its parents' values. This means that each probability distribution is conditionally independent of all its nondescendants in the graph given the values of its parent.

1) Description of Random Variables: mTBI, like most other injuries, evolves with time, so the contextual model (see Fig. 3) has multiple random variables that evolve with time. H_1 is the distribution of the time since the first injury. This random variable can be learned directly from the data or it can be modeled as an exponential distribution since it is most probable that a patient will arrive soon after the injury. Q is the random variable for the volume of injury over time. This distribution can also be learned from the data directly or modeled as a lognormal distribution. This distribution follows the natural progression of the injury where there is an initial peak in gross abnormality that resolves slowly overtime. As an example, Fig. 9(f) shows that gross pathology (in our data set) is maximal during the acute phase of the injury, followed by a sharp drop during the sub-acute phase and it approaches a steady state in the chronic phase. H_2 is the time between the first and second injury (i.e., repeated mTBI). After the first injury metabolic and cellular injury cascades occur which may lead to a window of vulnerability in which a second mTBI may worsen ongoing pathology [36]. This function can also be modeled directly from the data or using an exponential distribution from the time since first injury. The process of subsequent injuries can be thought of as a Poisson process, which has the time between injuries as an exponential distribution. H_1 and H_2 are variables that would be dependent on location and can be estimated through a regional epidemiological study.

2) Anatomical Constraints: Gross tissue level-pathology observed following mTBI may expand and contract throughout its
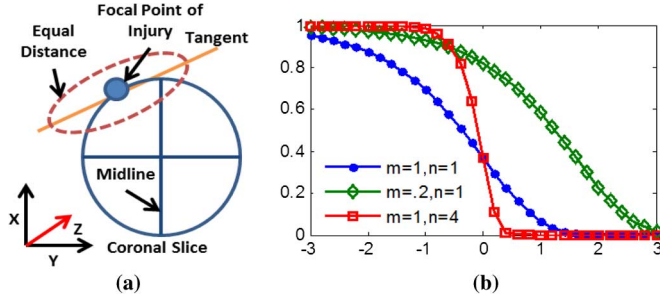
Fig. 4. (a) Description of the space and distance function. The XY plane is the coronal plane and the YZ is the sagittal plane. (b) Effect of parameters (m, n) on the Gompertz function, with the other parameters being held constant.
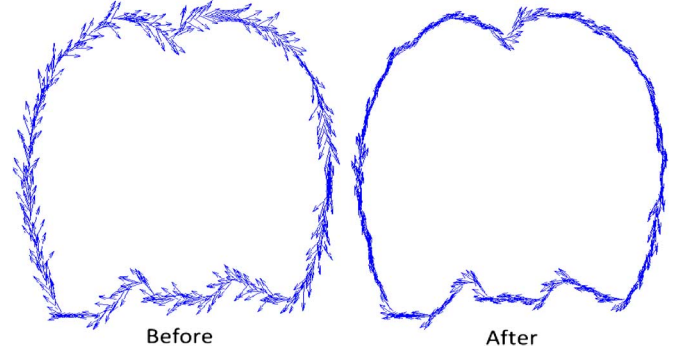

Fig. 5. Example of tangents around the perimeter of the brain. The tangents are scattered due to the low resolution of the boundary. The high-frequency noise is nullified after converting to the Fourier descriptor and filtering. The tangents are accurately estimated after filtering.

duration, but tissue structures provide natural barriers within the brain that restrict the spread of injury. For the rat brain model, two strong barriers are observed. The first boundary is the midline which is a physical separation between the left and right hemispheres. If the injury occurs on the left hemisphere it will not progress to the right. However, this may not be the case with severe and moderate injuries as the injury will extend throughout the brain. The second boundary that was observed is the major white matter tract (corpus callosum) that bounds the mild nature of the injury. To give an estimate of the location of the corpus callosum, the top 1/4th of the brain was used. These two constraints are represented in the form of a 3-D binary mask.

3) Location: An estimate of the location of the focal impact point is essential to modeling the progression of the injury. In our current model we account for two possible injury sites modeled by distributions L_1 and L_2. Examples of these distributions, estimated from our dataset, are shown in Fig. 9. Unlike other diseases that occur in specific locations/structures in the brain, mTBI progresses from an impact site which may occur at almost any point on the perimeter of the brain. To model the distribution of focal impact points, the perimeter distance in the coronal slices from the midline and the z location are used to make a 2-D distribution. The values are binned to make histograms. A smaller number of bins give a better generalization of the distributions when the sample size is small. When the sample size is larger the number of bins can be increased while maintaining a generalized distribution.

4) Spread: Equation (4) is used to describe the injury progression given all the contextual inputs. This function is a sigmoid like function, known as the Gompertz function [37], which has parameters (m, n) to control the shape and displacement. The Gompertz function has more flexibility than the logistic function and less number of parameters than the generalized logistic function. The effects of these parameters are shown in Fig. 4(b). Parameter m determines the displacement of the function and n determines the decay rate. The shape and displacement parameters are not the only variables that affect the shape of the curve; Q (quantity of lesion) also determines the shape. When Q is large, the function will shift to the right and have a more gradual slope. This represents a larger area for potential injury and more uncertainty in the location. When Q is small, the opposite is observed, the area is small and there is more certainty in the location. Q is estimated by taking the average le-

sion size at each time point for all the volumes in the database. There is a separate set of parameters for each H_2 value. This is due to the shape of the injury being different when the repeated injuries are at distinct times from each other. When the first hit occurs, there are many cellular cascades that take place throughout the progression of the injury potentially leaving the brain vulnerable to subsequent mTBIs [36]. This has been observed in animal models [36], [38]

$$p(S|L, A, H, Q) = Ae^{\frac{-m_H}{Q}e^{\frac{n_H}{Q}d(x,L)}}. \tag{4}$$

As described in (5), d is a distance function weighted by Σ. It measures the distance from L to every other point in the 3-D space. Σ weights the 3-D space so it accounts for rotation and scaling. The parameters described in (7)–(9) describe the rotation and scaling in the coronal space, and σ_z describes the scaling in the z space. The parameters that need to be set in these functions are σ_x and σ_y, which control the scaling in the direction of the tangent and the direction of the normal, respectively. Finding the tangent angle θ at L is done by utilizing the Fourier descriptor [39] of the closed perimeter of the brain slice. When converting to Fourier space a low pass filter is applied that cuts off the upper twenty percent of the frequencies (Fig. 5). The parameters, a, b and c control the rotation in the coronal plane using θ, to create the new "axis" for the distance function. Equation (4) models the progression of mTBI, since the injury spreads along the perimeter of the brain more than into the center of the brain. Hence, the distance function is weighted more along the tangent of the perimeter

$$d(x, L) = \sqrt{(x - L)^T \Sigma (x - L)} \tag{5}$$

$$\Sigma = \begin{bmatrix} a & b & 0 \\ b & c & 0 \\ 0 & 0 & \sigma_z \end{bmatrix} \tag{6}$$

$$a = \frac{\cos^2 \theta}{2\sigma_x^2} + \frac{\sin^2 \theta}{2\sigma_y^2} \tag{7}$$

$$b = \frac{\sin 2\theta}{4\sigma_x^2} + \frac{\sin 2\theta}{4\sigma_y^2} \tag{8}$$

$$c = \frac{\sin^2 \theta}{2\sigma_x^2} + \frac{\cos^2 \theta}{2\sigma_y^2}. \tag{9}$$
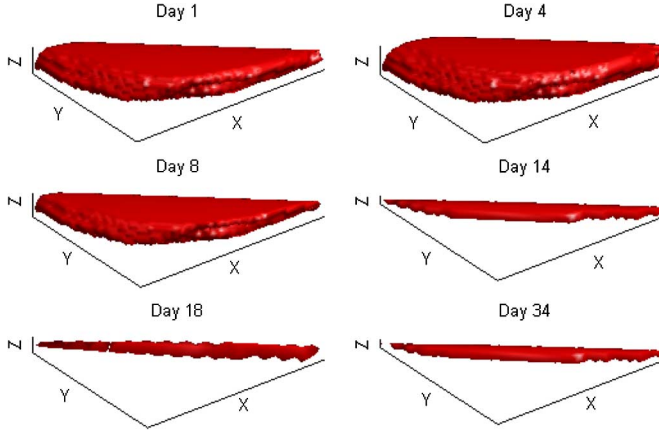
Fig. 6. An example of the contextual model over time. The surface is the model manually thresholded at 0.2 to give a solid surface that illustrates the progression of the model over time with all other variables constant. The XY plane is the coronal plane. Note, the best threshold for lesion detection is given as the threshold that maximizes the dice curve. An example of this is shown in Fig. 12.

The contextual model is finalized in (10). An example of the context over time is shown in Fig. 6. This function takes the maximum of the two spread functions evaluated over each value of the range of each contextual input. The output of the contextual model is an estimate of the lesion extent. If a contextual input is known then the probability of it being that value is 1. For example, if H_1 is known to be three days then $p(H_{1,3}) = 1$ and all other values in the distribution equal zero. Another example is when a ranged input is given. If H_1 is known to be between 5 and 14 days, the distribution becomes the priors known at those values normalized by the sum of the probabilities at those values (all other values are set to zero). If one of the contextual inputs is not known, all values in the prior distribution are considered

$$p(M|S_1, S_2) = \sum_{\forall i | (L_i) > 0,} \sum_{\forall j | P(Q_j) > 0,} \sum_{\forall k | P(H_{2k}) > 0}$$
$$\times \max \left(p(L_i)p(Q_j)p(H_{2k})p(S_{1ijk}), \right.$$
$$\left. p(L_i)p(Q_j)p(H_{2k})p(S_{2ijk}) \right) \quad (10)$$
$$p(I|M, V) = p(M)p(V). \quad (11)$$

An estimation of the lesion is finally given by (11). The contextual model and visual model are independent. This assumption has been made by other approaches using context [20]. The final output is a probability map.

5) Parameter Estimation: The parameters in the spread function (4) need to be learned. These parameters are learned from the known detected lesions in the database of mTBI volumes represented as a binary volume B, where 1 is lesion and 0 is NABM. r_{ij} is the set of variables [see (12)] that need to be learned in the spread function [see (4)] for each time of second impact (H_{2i}) and each anatomically constrained hemisphere A_j (left and right)

$$r_{ij} = [m_{ij}, n_{ij}, \sigma_{xij}, \sigma_{yij}, \sigma_{zij}]. \quad (12)$$

We use weighted nonlinear least squares [40], [41] to estimate the parameters. The cost function is given by

$$r_{ij} = \arg\min_{r_{ij}} \sum_{\forall B \in H_{2i} \wedge A_j} \omega \left(p(S_{r_{ij}}|L, A, H, Q) - B \right)^2$$
$$\text{where } \begin{cases} \omega = 1, & \text{if } B = 0 \\ \omega = \frac{\#\text{NABMVoxels}}{\#\text{LesionVoxels}}, & \text{if } B = 1 \end{cases}. \quad (13)$$

Each contextual input is known from the database for evaluating the spread function. Equation (13) finds an estimate $\widehat{r_{ij}}$ that minimizes the sum of the differences between the spread function ($S_{r_{ij}}$) and the ground truth (B) at every voxel. The weight ω is used to give the lesion a higher value in the cost function since there are many more NABM voxels compared to lesion voxels.

C. Visible Model

The visible model is the probability of an injury given the visual appearance of a sample voxel in the MRI. The MRI modality that has been chosen for evaluation of mTBI injury is T2WI and its quantitative T2 map. This modality allows for observation of both edema (increased signals) and extravascular blood (decreased signals), which are both potentially at the site of injury. Edema presents itself as high intensities and blood occurs as a low intensities. Note that we consider blood and edema as a single class. Since the edema and blood are believed to have local tissue effects, the texture around known lesions are used. The texture features that are used in this study are 3-D local mean, variance, skewness, kurtosis, entropy, range, gradient x, gradient y, gradient z. An example of these features can be seen in Fig. 7. These local statistics were chosen since they are able to describe small local neighborhoods at every voxel, which gives an estimate of the tissue. Note that partial voluming has less of an effect since the tissue is estimated and not a single voxel. The Bhattacharyya distance is a measure of the similarity of two distributions and can give a bound on the Bayesian error [42]. There are a total of ten features including the original T2 values. These features go through the feature selection process using the Bhattacharyya distance, to give the final feature set. The size of the filter is an important parameter and is found by finding the using the same feature selection process. The local neighborhood size found to be most discriminative is $5 \times 5 \times 5$. For our current dataset the features that are selected are: T2 value, entropy, variance, skewness, gradient x, T2 mean and gradient y.

SVMs are one of the leading supervised classifiers in machine learning. It is a max-margin classifier, which means it gives a decision boundary that maximizes the distance between the two classes. Describing the boundary using a maximum margin has been shown to provide a high generalization. The kernel form of SVM is utilized to give nonlinear boundaries. A radial basis function kernel is used to project the data to a high dimensional space making the separation linear. There are two parameters that need to be set when using the radial basis function, the soft margin parameter and the kernel shape parameter [44]. These two parameters are found through grid search that minimizes the error in a cross-validation test. SVM is generally used as a hard classifier with the output being one class or the other. However, Platt [43] proposed a framework for probabilistic SVM
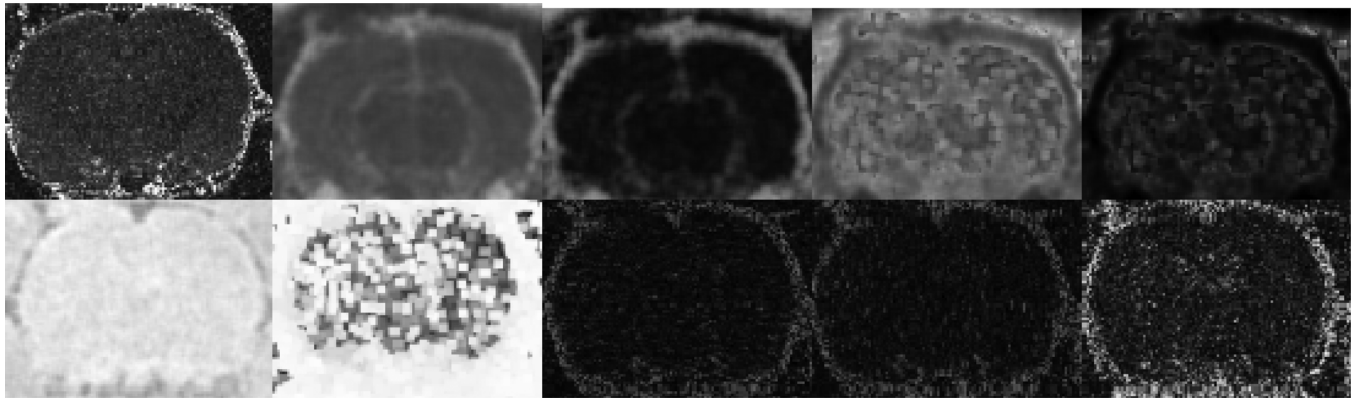
Fig. 7. Example of features with a 2-D coronal slice. Left to right, top to bottom: T2 map, mean, variance, skewness, kurtosis, entropy, range, gradient x, gradient y, gradient z
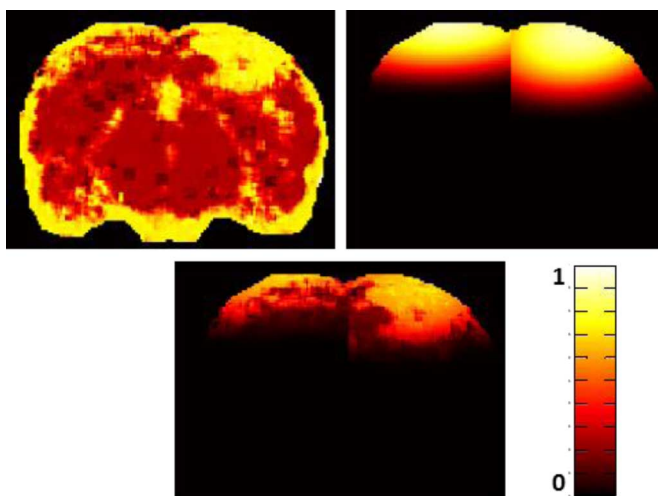

Fig. 8. Example of fusion between visual model and contextual model on a contralaterally injured rat. Top left: Probability map after PSVM. Top right: Probability map from the contextual model. Bottom: Fusion of the contextual and visual model. Note this shows that the contextual model for repeated injuries progress at different rates.

(PSVM) which allows for estimation of the posterior probability $p(\text{class}|\text{features})$. A sigmoid (with two parameters) is fit to the SVM result giving an estimate of the posterior probability for each class. Fig. 8 illustrates the estimates from the visual model and the fusion with the contextual model. LIBSVMs [44] implementation of PSVM is used for testing.

IV. Experimental Results

A. Dataset

Adult Sprague Dawley rats were randomly assigned to three experimental groups: Single mTBI, and repeated mTBI (rmTBI) induced three days or seven days apart. A controlled cortical impact (CCI) was used to induce mild injury [6], [45]. The CCI model has a focal injury. Briefly, a craniectomy (5 mm) was performed over the right hemisphere (3 mm lateral, 3 mm posterior to bregma) where a mild CCI was induced using an electromagnetically driven piston (4 mm diameter, 0.5 mm depth, 6.0 m/s). The incision made for the craniectomy is sutured after the injury is induced. At three or seven days after the initial injury, animals within the rmTBI groups (repeated injury) received a

second craniotomy and mCCI was induced on the left hemisphere using identical parameters.

In vivo T2 weighted images (T2WI) were collected as multiple 2-D slices [6]. Images were obtained at 1, 4, 8, 14, 21, 30, and 60 days postinitial injury using a 4.7T Bruker Avance (Bruker Biospin, Billerica, MA, USA). T2WI sequences (TR/TE = 3453 ms/20 ms; 25 × 1 mm slice) were collected with a field-of-view of 3 cm (256 × 256 matrix). The resolution of each voxel is 0.12 × 0.12 × 1 mm. On average 12 coronal slices were used to cover the cerebrum. T2 maps were computed using custom written software. Regions-of-interest (ROIs) were manually drawn using Cheshire imaging software (Haydan Image/Processing Group) [45]. ROIs included normal appearing brain matter (NABM) and cortical tissue containing T2 observable abnormalities using criteria from [45]. There were a total of 81 volumes in the dataset with time points, as shown in Fig. 9(e). Manual outlines of the brain were used to separate the brain from the skull and other tissues.

B. Performance Measures

To provide a sense of where errors are coming from and how the regions are correctly detected, the following measures were used. *Sensitivity* or true positive rate (TPR) (14) measures the percentage of the target object that is correctly detected. *Specificity* or true negative rate (15) is the percentage of the background that is correctly detected. 1-Specificity gives the false positive rate (FPR), which is the false alarm rate. A *receiver operating characteristic* (ROC) curve is shown for each of the tests. A threshold is set on the probability map output from the algorithm to give a binary decision surface. Each threshold creates a point on the ROC curve and together they form a graph that represents the tradeoff between TPR and FPR. ROC has been a strong measure of performance in radiology and other medical disciplines [46]. Only FPR under 0.2 are considered for clinical relevance

$$\text{sensitivity} = \frac{\text{TP}}{\text{TP} + \text{FN}} \qquad (14)$$

$$\text{specificity} = \frac{\text{TN}}{\text{TN} + \text{FP}} \qquad (15)$$

$$\text{Dice} = \frac{2\text{TP}}{(\text{TP} + \text{FP}) + (\text{TP} + \text{FN})}. \qquad (16)$$
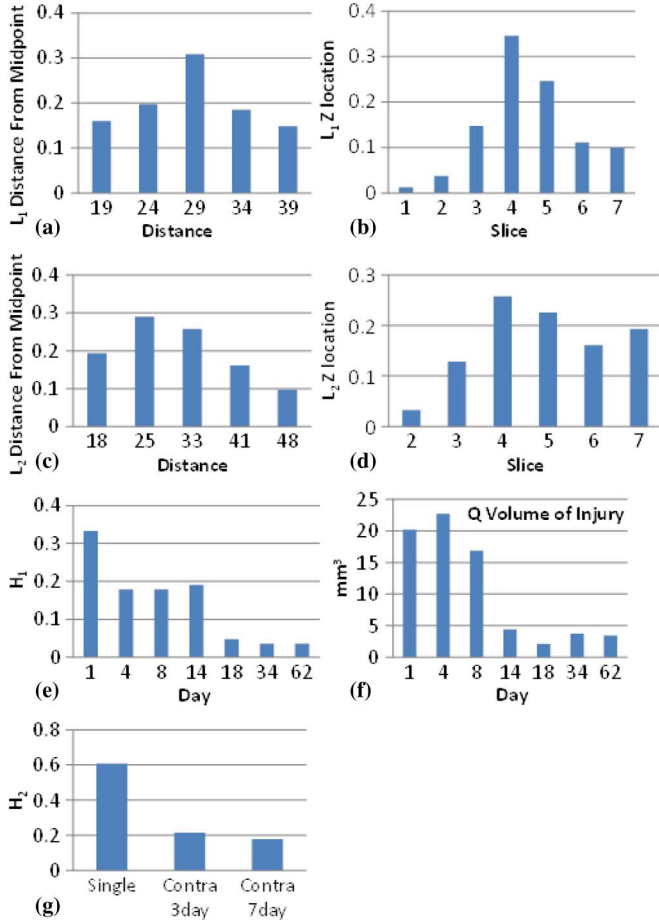
Fig. 9. Distributions learned from the database for each of the nodes in the Bayesian network. Note the number of bins used in: (a) and (c) is 5, (d) is 6, and (b), (e), (f) is 7.
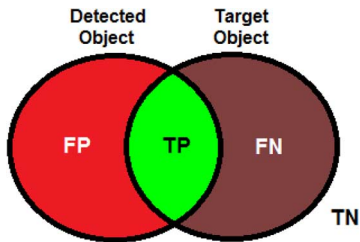

Fig. 10. Visual meaning of measurements. FPL: False positive. TP: True positive. FN: False negative. TN: True negative.

The *Dice coefficient* (16) measures set agreement, which is the intersection of the known object and the detected object divided by the size of the known and detected objects. Dice gives a better idea of the intersection between the detected object and the actual object since it does not include true negatives in the calculation. Fig. 10 shows the physical meaning of theses performance measures.

C. Varying Levels of Context

In these experiments each contextual input was tested to verify the effects they have on the model using our real data. Testing was conducted using the leave-one-out approach for learning the parameters. The following cases were examined: all contexts known, L_1 and L_2 unknown position (unkPOS), H_1 unknown time (unkTIME), $L_1 L_2 H_1$ unknown (unkALL), and V alone (Probabilistic SVM). Fig. 11 is the ROC plot for
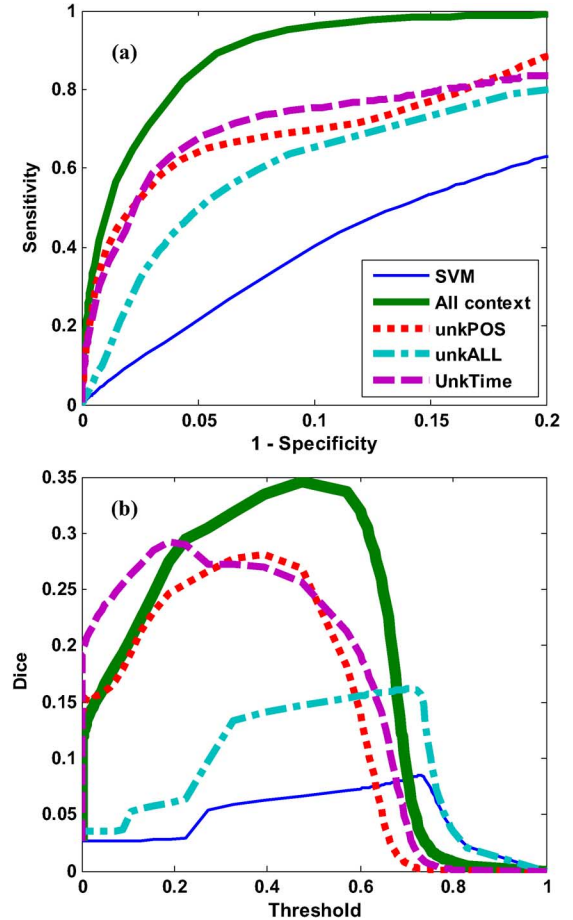

Fig. 11. (a) ROC plot with multiple contextual inputs. Results were evaluated after thresholding the output probability map [from (11)]. (b) Dice plot with multiple contextual inputs. The peak of the Dice curve (maximum dice coefficient) is used to threshold the output probability map. Legends in (b) are the same as in (a).

each of the aforementioned context tests after thresholding the output probability maps to get a hard classification. When all the context is known an equal error rate of 0.93 is achieved, and with missing context a decrease in performance is obtained.

The Dice plot in Fig. 11 shows results corresponding to the results in the ROC plot. With unkPOS and unkTIME a similar performance is observed since each of these cases causes a smoothing effect in the output of the contextual model. This smoothing effect is clearly seen in Fig. 12. Essentially, when the context is not known, a wider area has to be considered. In the case of unkPOS smoothing is experienced along the edges of a brain since the focal point is shifted along the perimeter of the brain. The unkTIME case has smoothing in all directions, which is due to the time points with a large amount of lesion having the largest effect on the output from the contextual model. In unkALL both of the smoothing effects occur.

D. Class Analysis

Evaluating the performance of each class (single, contra3, contra7) gives an insight into the potential errors of the model. From Fig. 13 it is clear that the single mTBI class has the best performance. This is due to the single mTBI class being more consistent allowing the model to estimate the area of injury
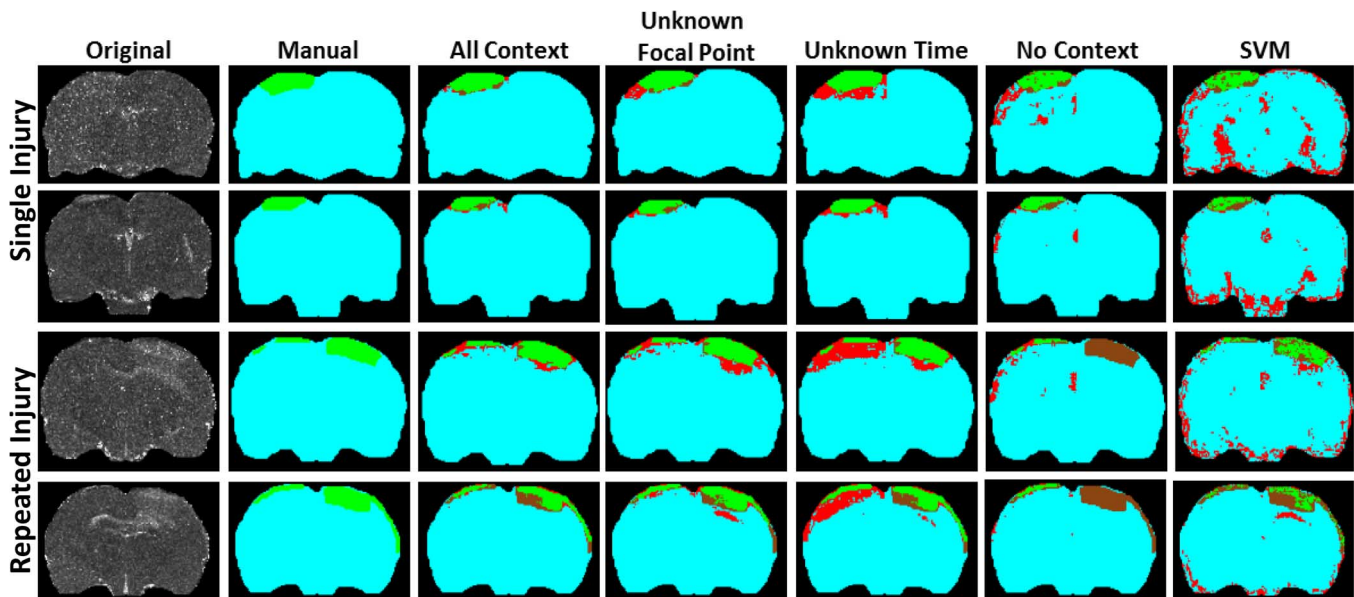
Fig. 12. Example outputs from the thresholded probability maps (for single and repeated mTBI) with varying levels of contextual input. The thresholds are selected at the highest point on the dice curve for each respective level of context. Each row is a coronal slice, where the top two are from a single mTBI rat and the bottom two are from a repeated mTBI rat. The colors represent the following. Green: True positive. Teal: True negative. Red: False positive. Brown: False negative. (Note: This figure should be viewed in color.)

better. The distributions for L_2 [in Fig. 9(c)] show that the second injury is less consistent than the first. Also, there is more variation in the shape and size of the second mTBI.

E. Ranged Context

In this test the effect of having ranged values for contextual input is examined. The known locations are first binned into the distribution shown in Fig. 9(a)–(d). From the known location a range of values is obtained by taking a set number of bins on either side of the known location (Fig. 14). For example, if L_1 is known to be 29 voxels from the midline and the range input is to be two steps away, the range input would be from 19–39 voxels from the midline [values from Fig. 9(a)]. The results from range testing are shown in Fig. 15. From these plots it is evident that the performance increases as the position is closer to the known location. As the range gets wider the result approaches the performance of having the position unknown. This is due to the contextual model being able to focus when the values are known and hence follow the progression of the injury better. Ranged values are possible inputs to the system and give better performance than having completely unknown inputs.

F. Comparison With State-of-the-Art Approaches

The proposed approach is compared to two other state-of-the-art approaches. The compared approaches are setup as described in the papers [22], [24]. First, the approach of Sun *et al.* [24] is used since it is a purely data driven approach, which does not account for contextual or database information. This approach uses symmetry to find asymmetric lesions in the brain. This approach does not use any prior knowledge of the brain except that it should be symmetric. The user set parameters were optimized using three example T2 maps from the dataset, and

then the parameters were fixed for testing of the entire dataset. The second approach that was chosen to compare against is that of Anbeek *et al.* [22]. Their approach is pure model-based approach, which takes advantage of visual information in the database. The volumes are registered, with rigid registration, and then a KNN model is built from the known lesions in the dataset. Since unimodal MRI data are used, the texture features are used in their approach as channels. The parameters were chosen as described in [22] and each feature was normalized.

The results from Table II demonstrate that the performance of our proposed approach outperforms the compared state-of-the-art approaches. All of the approaches tend to underestimate the lesion area [24], had difficulty in detecting the mTBI lesions due to the subtle T2 value differences and the lesions were mostly comprised of textured area. These two problems caused [24] to consider lesion within NABM. The symmetry approach [24] is best suited for stroke data where the lesions are more uniform and have higher contrast. The pure model-based approach [22] also had difficulties due to the low number of lesion voxels and the injury not occurring within the same locations consistently. A large amount of data is required for a viable K-NN classifier and the lesions must occur in a similar location. MS is a disease where the model-based approach [22] excels since the lesions are primarily identified in the white matter locations. Also, a proper ratio between diseased brains and normal brains would have to be maintained to give a proper normal versus abnormal bias.

Run time is also a consideration when determining the effectiveness of an algorithm. All testing was carried out on the same computer system (PC with Intel Xeon (E5345) Quad CPU 2.33 GHz and 2 GB of RAM). The proposed contextual and visual approach has the fastest computation time. A majority of the time is spent in the PSVM calculation. The pure model-based approach [22] had increased computation time, due to
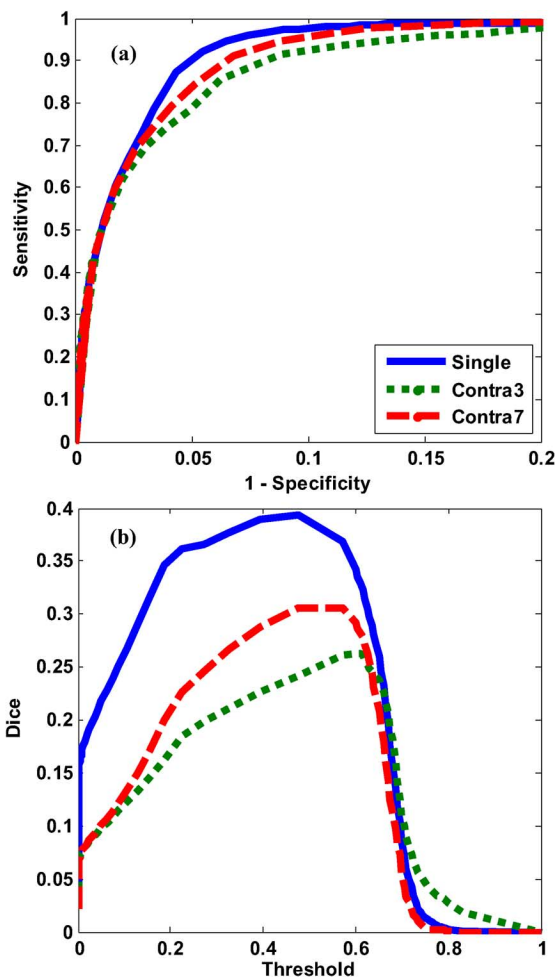
Fig. 13. (a) ROC for each class. (b) Dice plot for each class. Definition of classes: Single-only a single injury, Contra3-contralateral injury three days after the first injury, Contra7-contralateral injury seven days after the first injury. Legends of (a) and (b) are the same.

Fig. 14. Example of the ranged inputs on H_1. The midline is shown in yellow. Orange (arrow) is the focal impact point, blue −1 away, green −2 away, red −3 away. Each higher range includes the previous. For example, 2 away includes 1 away. Increasing the away, increases the uncertainty in the position. It represents including the value in the prior histogram [Fig. 9(e)] some step away (left and right) of the true point.

each sample needing to be compared to every sample in the database. Some increases in speed could be made to the K-NN algorithm, but when the database becomes large computation time will become large.

G. Applicability of the Proposed Approach to Human Data

In this paper, we showed single and multiple injuries over time as follows. 1) Our model accepts an input as a brain volume with contextual information at a single point in time as an input. Multiple volumes are not need to ensure an accurate estimate. 2) The location of the injury may be focal, diffuse or unknown.
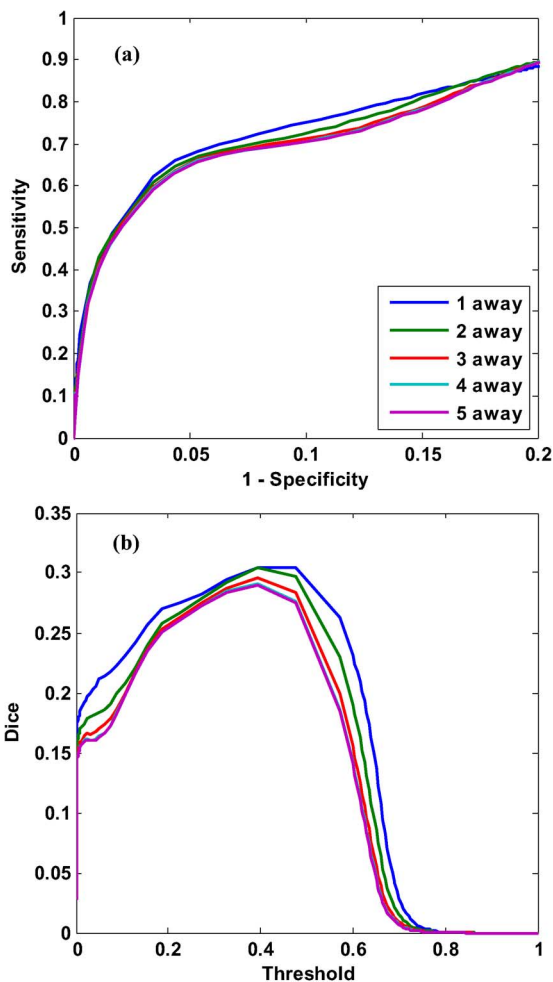

Fig. 15. (a) ROC plot with varying distance input. (b) Dice for varying input distance. Legends of (a) and (b) are the same.

TABLE II
COMPARISON OF ALGORITHMS

Method	TPR	FPR	Dice	Time
Sun [24]	0.06 (0.01-0.11)	0.003 (0.0-0.015)	0.02 (0.0-0.05)	~10min
Anbeek [22]	0.07 (0.01-0.13)	0.002 (0.0-0.012)	0.13 (0.057-0.203)	~24hrs
PSVM (*)	0.73 (0.63-0.83)	0.27 (0.173-0.367)	0.07 (0.014-0.125)	~4mins
Proposed (*)	0.93 (0.87-0.99)	0.07 (0.014-0.126)	0.25 (0.156-0.344)	~5mins
Proposed (**)	0.57 (0.46-0.68)	0.015 (0.0-0.041)	0.35 (0.246-0.453)	~5mins

Time is in the online phase of the algorithm. The range (−) is the 95% confidence interval. (*—at the equal error rate, **—at the highest dice). The time is for an entire brain.

If the location is unknown then prior distributions L_1 and L_2 (shown in Fig. 9) are used as possible locations, where each location is tested and weighted by the distribution. If the injured region is diffuse then a ranged input can be given (as shown in Section IV-E). 3) We have focused on focal lesions in this paper. Note that for diffuse lesions it is extremely difficult to get ground truth and one has to rely in histological data. This topic will be explored further in the future. 4) Multiple lesions can

be handled by our approach (see Fig. 12). Over time the lesions may collapse into a single lesion or break into multiple lesions. These lesions can be detected using visual and contextual modeling. The model will need to be updated for cases where there are more than two injuries.

V. CONCLUSION

An approach was presented that incorporates visual and contextual knowledge to detect mTBI lesions using unimodal MRI, specifically T2 maps. Texture features are used with Probabilistic SVM to create a visual model of the mTBI appearance on the T2 MRI maps. The contextual model utilizes a Bayesian network which allows for exact or partial contextual inputs to be given to the system. Qualitative and quantitative results of the algorithm were shown using a novel rat mTBI dataset. The results show when more contexts are known, we obtain injury detections that are highly similar to the manually detected lesions by a trained observer. An equal error rate of 0.93 was achieved. The proposed algorithm outperformed other state-of-the-art-approaches, including computation time performance. This work will be extended to human data through the use of large mTBI databases and some modification. New animal models will be explored that include diffuse and contra coup injuries. Integration of susceptibility weighted imaging and diffusion tensor imaging is expected to improve the performance of the visual modeling and improve the contextual model through the estimation of WM tracts.

REFERENCES

[1] T. Morris, "Traumatic brain injury," in *Handbook of Medical Neuropsychology*, C. L. Armstrong and L. Morrow, Eds. New York: Springer, 2010, ch. 2, pp. 17–32.

[2] 2002, Center for Disease Control and Prevention, Heads Up: Facts for physicians about mild traumatic brain injury (MTBI) [Online]. Available: http://www.cdc.gov/ncipc/tbi/TBI.htm

[3] R. C. Cantu, "Second-impact syndrome," *Clin. Sports Med.*, vol. 17, no. 1, pp. 37–44, 1998.

[4] D. Cifu *et al.*, "VA/DoD Clincial practice guideline for management of concussion/mild traumatic brain injury," *J. Rehabil. Res. Develop.*, vol. 46, no. 6, pp. CP1–CP68, 2009.

[5] N. C. Colgan, M. M. Cronin, O. L. Gobbo, S. M. O'Mara, W. T. O'Connor, and M. D. Gilchrist, "Quantitative MRI analysis of brain volume changes due to controlled cortical impact," *Neurotrauma*, vol. 27, no. 7, pp. 1265–1274, July 2010.

[6] A. Obenaus, M. Robbins, G. Blanco, N. R. Galloway, E. Snissarenko, E. Gillard, S. Lee, and M. Currás-Collazo, "Multi-modal magnetic resonance imaging alterations in two rat models of mild neurotrauma," *Neurotrauma*, vol. 24, no. 7, pp. 1147–1160, Jul. 2007.

[7] Z. Metting, L. A. Rodiger, J. De Keyser, and J. Van Der Naalt, "Structural and functional neuroimaging in mild-to-moderate head injury," *Lancet Neurol.*, vol. 6, no. 8, pp. 699–710, Aug. 2007.

[8] G. P. Mazzara, R. P. Velthuizen, J. L. Pearlman, H. M. Greenberg, and H. Wagner, "Brain tumor target volume determination for radiation treatment planning through automated MRI segmentation," *Int. J. Radiat. Oncol. Biol. Phys.*, vol. 59, no. 1, pp. 300–312, May 2004.

[9] T. Niimi, K. Imai, H. Maeda, and M. Ikeda, "Information loss in visual assessments of medical images," *Eur. J. Radiol.*, vol. 61, no. 2, pp. 362–366, Feb. 2007.

[10] K. A. Tong, "New MRI techniques for imaging of head trauma: DWI, MRS, SWI," *Appl. Radiol.*, vol. 32, no. 7, pp. 29–34, Jul. 2003.

[11] I. Kharatishvili, A. Sierra, R. J. Immonen, O. H. J. Gröhn, and A. Pitkänen, "Quantitative T2 mapping as a potential marker for the initial assessment of the severity of damage after traumatic brain injury in rat," *Exp. Neurol.*, vol. 217, no. 1, pp. 154–164, May 2009.

[12] J. Rajan, D. Poot, J. Juntu, and J. Sijbers, "Noise measurement from magnitude MRI using local estimates of variance and skewness," *Phys. Med. Biol.*, vol. 55, no. 16, p. N441, Aug. 2010.

[13] A. Irimia, M. C. Chambers, J. R. Alger, M. Filippou, M. W. Prastawa, B. Wang, D. A. Hovda, G. Gerig, A. W. Toga, R. Kikinis, P. M. Vespa, and J. D. Van Horn, "Comparison of acute and chronic traumatic brain injury using semi-automatic multimodal segmentation of MR volumes," *J. Neurotrauma*, vol. 28, no. 11, pp. 2287–2306, Nov. 2011.

[14] R. de Boer, H. A. Vrooman, F. Van Der Lijn, M. W. Vernooij, M. A. Ikram, A. Van Der Lugt, M. M. B. Breteler, and W. J. Niessen, "White matter lesion extension to automatic brain tissue segmentation on MRI," *NeuroImage*, vol. 45, no. 4, pp. 1151–1161, May 2009.

[15] J. M. Fitzpatrick, J. B. West, J. Maurer, and C. R. , "Predicting error in rigid-body point-based registration," *IEEE Trans. Med. Imag.*, vol. 17, no. 5, pp. 694–702, May 1998.

[16] P. Thevenaz, T. Blu, and M. Unser, "Interpolation revisited [medical images application]," *IEEE Trans. Med. Imag.*, vol. 19, no. 7, pp. 739–758, Jul. 2000.

[17] F. Kruggel, J. S. Paul, and H.-J. Gertz, "Texture-based segmentation of diffuse lesions of the brain's white matter," *NeuroImage*, vol. 39, no. 3, pp. 987–996, Feb. 2008.

[18] S. Ahmed, K. M. Iftekharuddin, and A. Vossough, "Efficacy of texture, shape, and intensity feature fusion for posterior-fossa tumor segmentation in MRI," *IEEE Trans. Inf. Technol. Biomed.*, vol. 15, no. 2, pp. 206–213, Mar. 2011.

[19] K. Holli, L. Harrison, P. Dastidar, M. Waljas, S. Liimatainen, T. Luukkaala, J. Ohman, S. Soimakallio, and H. Eskola, "Texture analysis of MR images of patients with mild traumatic brain injury," *BioMedCentral Med. Imag.*, vol. 10, no. 8, May 2010.

[20] O. Marques, E. Barenholtz, and V. Charvillat, "Context modeling in computer vision: Techniques, implications, and applications," *Multimedia Tools Appl.*, vol. 51, no. 1, pp. 303–339, Jan. 2011.

[21] C. Galleguillos and S. Belongie, "Context based object categorization: A critical survey," *Comput. Vis. Image Understand.*, vol. 114, no. 6, pp. 712–722, Jun. 2010.

[22] P. Anbeek, K. L. Vincken, M. J. P. Van Osch, R. H. C. Bisschops, and J. Van Der Grond, "Automatic segmentation of different-sized white matter lesions by voxel probability estimation," *Med. Image Anal.*, vol. 8, no. 3, pp. 205–215, Sep. 2004.

[23] N. Zhang, S. Ruan, S. Lebonvallet, Q. Liao, and Y. Zhu, "Kernel feature selection to fuse multi-spectral MRI images for brain tumor segmentation," *Comput. Vis. Image Understand.*, vol. 115, no. 2, pp. 256–269, Feb. 2011.

[24] Y. Sun, B. Bhanu, and S. Bhanu, "Automatic symmetry-integrated brain injury detection in MRI sequences," in *Proc. IEEE Comput. Soc. Conf. Comput. Vis. Pattern Recognit.*, Jun. 2009, pp. 79–86.

[25] M. L. Seghier, A. Ramlackhansingh, J. Crinion, A. P. Leff, and C. J. Price, "Lesion identification using unified segmentation-normalisation models and fuzzy clustering," *NeuroImage*, vol. 41, no. 4, pp. 1253–1266, Jul. 2008.

[26] S. K. Divvala, D. Hoiem, J. H. Hays, A. A. Efros, and M. Hebert, "An empirical study of context in object detection," in *Proc. IEEE Cong. Comput. Vis. Pattern Recognit.*, Miami, FL, 2009, pp. 1271–1278.

[27] M. J. Choi, A. Torralba, and A. S. Willsky, "A tree-based context model for object recognition," *IEEE Trans. Pattern Anal. Mach. Intell.*, vol. 34, no. 2, pp. 240–252, Feb. 2012.

[28] A. Rabinovich, A. Vedaldi, C. Galleguillos, E. Wiewiora, and S. Belongie, "Objects in context," in *Proc. IEEE Int. Conf. Comput. Vis.*, Rio de Janeiro, Brazil, 2007, pp. 1–8.

[29] C. Galleguillos, A. Rabinovich, and S. Belongie, "Object categorization using co-occurrence, location and appearance," in *Proc. IEEE Cong. Comput. Vis. Pattern Recognit.*, Anchorage, AK, Jun. 2008, pp. 1–8.

[30] R. Perko and A. Leonardis, "A framework for visual-context-aware object detection in still images," *Comput. Vis. Image Understand.*, vol. 114, no. 6, pp. 700–711, Jun. 2010.

[31] A. Torralba, K. P. Murphy, and W. T. Freeman, "Using the forest to see the trees: Exploiting context for visual object detection and localization," *Commun. ACM*, vol. 53, no. 3, pp. 107–114, Mar. 2010.

[32] Z. Tu and X. Bai, "Auto-context and its application to high-level vision tasks and 3-D brain image segmentation," *IEEE Trans. Pattern Anal. Mach. Intell.*, vol. 32, no. 10, pp. 1744–1757, Oct. 2010.

[33] M. A. Horsfield, R. Bakshi, M. Rovaris, M. A. Rocca, V. S. R. Dandamudi, P. Valsasina, E. Judica, F. Lucchini, C. R. G. Guttmann, M. PiaSormani, and M. Filippi, "Incorporating domain knowledge into the fuzzy connectedness framework: Application to brain lesion volume estimation in multiple sclerosis," *IEEE Trans. Med. Imag.*, vol. 26, no. 12, pp. 1670–1680, Dec. 2007.

[34] A. Bianchi, B. Bhanu, V. Donovan, and A. Obenaus, "Contextual and visual modeling for detection of mild traumatic brain injury in MRI," in *IEEE Int. Conf. Image Process.*, Orlando, FL, Oct. 2012, pp. 1261–1264.

[35] M. Kafai and B. Bhanu, "Dynamic Bayesian networks for vehicle classification in video," *IEEE Trans. Ind. Informat.*, vol. 8, no. 1, pp. 100–109, Feb. 2012.

[36] R. Vagnozzi, B. Tavazzi, S. Signoretti, A. M. Amorini, A. Belli, M. Cimatti, R. Delfini, V. Di Pietro, A. Finocchiaro, and G. Lazzarino, "Temporal window of metabolic brain vulnerability to concussions: Mitochondrial-related impairment—Part I," *Neurosurgery*, vol. 61, no. 2, pp. 379–388, Aug. 2007.

[37] A. K. Laird, "Dynamics of tumor growth," *Br. J. Cancer*, vol. 18, no. 3, pp. 490–502, Sep. 1964.

[38] L. Longhi, K. E. Saatman, S. Fujimoto, R. Raghupathi, D. F. Meaney, J. Davis, B. S. A. McMillan, V. Conte, H. L. Laurer, S. Stein, N. Stocchetti, and T. K. McIntosh, "Temporal window of vulnerability to repetitive experimental concussive brain injury," *Neurosurgeryvol.*, vol. 56, no. 2, pp. 364–374, Feb. 2005.

[39] L. F. Costa and R. M. Cesar, *Shape Analysis and Classification: Theory and Practice.* Boca Raton, FL: CRC, 2001.

[40] T. F. Coleman and Y. Li, "An interior, trust region approach for nonlinear minimization subject to bounds," *SIAM*, vol. 6, no. 2, pp. 418–445, Jul. 1996.

[41] T. F. Coleman and Y. Li, "On the convergence of reflective newton methods for large-scale nonlinear minimization subject to bounds," *Math. Programm.*, vol. 67, no. 2, pp. 189–224, 1994.

[42] X. Guorong, C. Peiqi, and W. Minhui, "Bhattacharyya distance feature selection," in *Proc. Int. Conf. Pattern Recognit.*, Vienna, Austria, 1996, pp. 195–199.

[43] J. C. Platt, "Probabilistic outputs for support vector machines and comparison to regularized likelihood methods," in *Advances in Large Margin Classifiers.* Cambridge, MA: MIT Press, 2000, pp. 61–74.

[44] C. C. Chang and C. J. Lin, "LIBSVM: A library for support vector machines," *ACM Trans. Intell. Syst. Technol.*, vol. 2, no. 3, pp. 1–39, 2011.

[45] V. Donovan, A. Bianchi, R. Hartman, B. Bhanu, M. J. Carson, and A. Obenaus, "Computational analysis reveals increased blood deposition following repeated mild traumatic brain injury," *NeuroImage: Clinical*, vol. 1, no. 1, pp. 18–28, 2012.

[46] N. A. Obuchowski, "Receiver operating characteristic curves and their use in radiology," *Radiology*, vol. 229, no. 1, pp. 3–8, 2003.